

Tuning upconversion through energy migration in core-shell nanoparticles

Feng Wang¹, Renren Deng¹, Juan Wang¹, Qingxiao Wang², Yu Han², Haomiao Zhu³, Xueyuan Chen³ and Xiaogang Liu^{1,4,5}★

Photon upconversion is promising for applications such as biological imaging, data storage or solar cells. Here, we have investigated upconversion processes in a broad range of gadolinium-based nanoparticles of varying composition. We show that by rational design of a core-shell structure with a set of lanthanide ions incorporated into separated layers at precisely defined concentrations, efficient upconversion emission can be realized through gadolinium sublattice-mediated energy migration for a wide range of lanthanide activators without long-lived intermediary energy states. Furthermore, the use of the core-shell structure allows the elimination of deleterious cross-relaxation. This effect enables fine-tuning of upconversion emission through trapping of the migrating energy by the activators. Indeed, the findings described here suggest a general approach to constructing a new class of luminescent materials with tunable upconversion emissions by controlled manipulation of energy transfer within a nanoscopic region.

Anti-Stokes emission processes that convert long-wavelength pump sources into short-wavelength emission have recently attracted great attention in diverse research fields, not only for their fundamental scientific importance but also because of their potential applications, ranging from compact solid-state lasers and optical data storage to biological imaging and solar energy conversion^{1–5}. Simultaneous two-photon absorption (TPA) is a well-established method for generating anti-Stokes emissions from a host of luminescent materials such as organic dyes and semiconducting nanoparticles (Fig. 1a; refs 6,7). Alternatively, second-harmonic generation (SHG) can be used to perform anti-Stokes conversion (Fig. 1b; refs 8,9). However, there are inherent limitations associated with these two methods with regard to the requirement of either expensive pulsed lasers with high-density excitation (10^6 – 10^9 W cm⁻²) or nonlinear optical materials with a non-centrosymmetric atomic or molecular organization.

Upconversion, typically classified by excited state absorption (ESA) or energy transfer upconversion (ETU) through the use of physically existing intermediary energy states of lanthanide ions (Fig. 1c,d), has emerged as an attractive alternative for the generation of anti-Stokes emissions^{11,10}. This method encompasses the benefit of high conversion efficiency without the need for intense coherent excitation sources, with the inherent advantages of large anti-Stokes shifts, sharp emission bandwidths, and long excited-state lifetimes. The ability to prepare small-sized lanthanide-doped nanoparticles with high photostability and low cytotoxicity has enabled them to be particularly suitable for biological labelling and imaging applications^{11–39}. Despite these attractions, efficient upconversion is generally restricted to Er³⁺, Tm³⁺ and Ho³⁺ activators, characterized by ladder-like arranged energy levels essential for facilitating the successive photon absorption and energy transfer steps¹¹. The challenge of upconversion in other ion systems has been met with limited success since the discovery of upconversion in the mid-1960s (ref. 10).

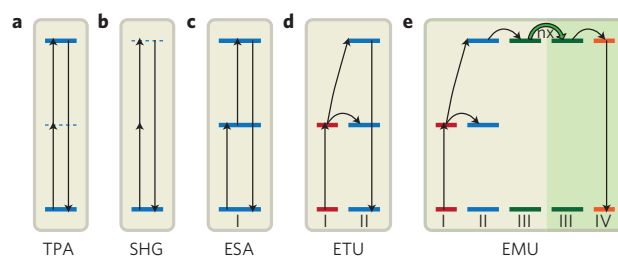


Figure 1 | Simplified energy level diagrams depicting reported and proposed anti-Stokes processes. a, TPA scheme showing simultaneous absorption of two photons without involving any real intermediary energy level. **b**, SHG (also called frequency doubling) scheme showing the frequency of irradiated light is doubled without any absorption transition taking place. **c**, Upconversion by an ESA scheme on a single lanthanide ion in which two photons are sequentially absorbed using a real intermediary energy level. **d**, ETU scheme involving two types of lanthanide ions in which one ion successively transfers its excitation energy to a neighbouring ion that can emit from a high energy level. **e**, The proposed EMU scheme involving the use of four types of lanthanide ions and a core-shell design. Note that core and shell regions are highlighted with different background colours. A sensitizer ion (type I) first transfers its excitation energy to an accumulator ion (type II). The energy transfer from the high-lying excited state of the accumulator to a migrator ion (type III) then occurs, followed by the migration of excitation energy via the migrator ion sublattice through the core-shell interface. Subsequently, the migrating energy is trapped by the activator ion (type IV), resulting in upconverted emission. The 'nx' denotes the occurrence of random hopping through many type-III ions.

Herein, we describe an experimental investigation of photon upconversion in core-shell nanoparticles doped with a series of lanthanide ions. For a variety of lanthanide activators without long-lived intermediary energy states, we demonstrated that tunable

¹Department of Chemistry, National University of Singapore, 117543, Singapore, ²Advanced Membrane and Porous Materials Center & Imaging and Characterization Core Lab, King Abdullah University of Science and Technology, Thuwal 23955-6900, Saudi Arabia, ³Key Laboratory of Optoelectronic Materials Chemistry and Physics, Fujian Institute of Research on the Structure of Matter, Chinese Academy of Sciences, Fuzhou, Fujian 350002, China, ⁴Institute of Materials Research and Engineering, 3 Research Link, 117602, Singapore, ⁵Singapore-MIT Alliance, 4 Engineering Drive 3, 117576, Singapore. ★e-mail: chmlx@nus.edu.sg.

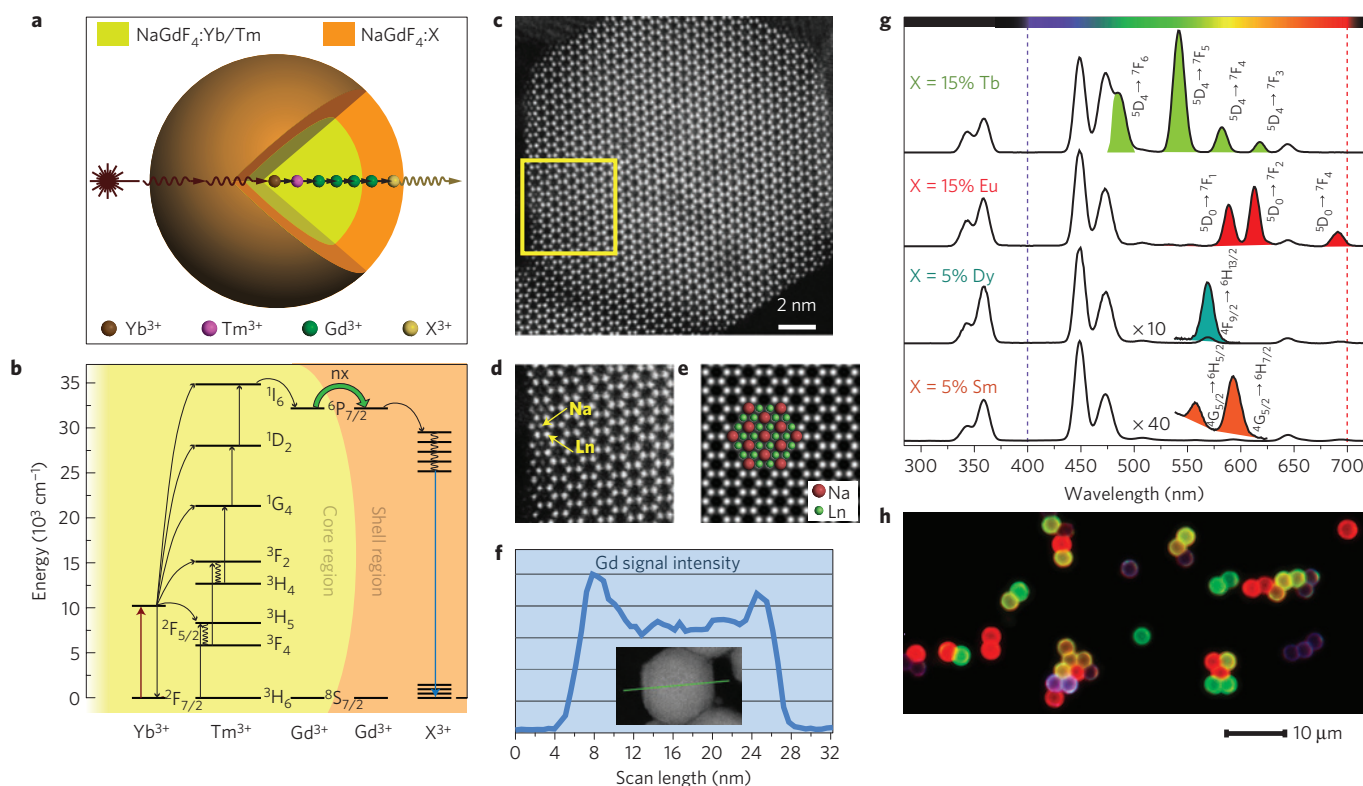


Figure 2 | Tuning upconversion through energy migration in core-shell nanoparticles. **a**, Schematic design of a lanthanide-doped $\text{NaGdF}_4/\text{NaGdF}_4$ core-shell nanoparticle for EMU (X: activator ion). **b**, Proposed energy transfer mechanisms in the core-shell nanoparticle. Note that only partial energy levels of Tm^{3+} and Gd^{3+} are shown for clarity. **c**, High-resolution STEM image taken at [001] incidence of a nanoparticle comprising a $\text{NaGdF}_4/\text{Yb/Tm}$ (49/1%) core and a NaGdF_4/Tb (15%) shell, revealing the single-crystalline nature of the crystal. **d**, An enlarged view of the selected area in **c**, indicated by a yellow box, showing lanthanide (Ln) and Na atomic columns. **e**, Digitally processed STEM image by imposing projection symmetry to enhance the signal-to-noise ratio. **f**, EELS line scan conducted with STEM imaging (inset) on a $\text{NaGdF}_4/\text{Yb/Tm}$ (49/1%) @ NaGdF_4/Tb (15%) nanoparticle, indicating a higher Gd concentration in the peripheral region of the crystal that is very consistent with the designed core-shell structure. **g**, Emission spectra of the as-prepared $\text{NaGdF}_4/\text{NaGdF}_4$ core-shell nanoparticles doped with different activators (activator emissions are highlighted with colour). **h**, Luminescence micrograph of polystyrene beads tagged with core-shell nanoparticles comprising $\text{NaGdF}_4/\text{Yb/Tm}/\text{NaGdF}_4$ (blue), $\text{NaGdF}_4/\text{Yb/Tm}/\text{NaGdF}_4/\text{Tb}$ (green), $\text{NaGdF}_4/\text{Yb/Tm}/\text{NaGdF}_4/\text{Eu}$ (red), and a binary mixture of $\text{NaGdF}_4/\text{Yb/Tm}/\text{NaGdF}_4/\text{Tb}$ and $\text{NaGdF}_4/\text{Yb/Tm}/\text{NaGdF}_4/\text{Eu}$ (yellow), respectively.

upconversion emissions can be achieved by controlling gadolinium (Gd) sublattice-mediated energy migration^{40–42} through a well-defined core-shell structure. The lanthanide ions designed for realizing energy migration-mediated upconversion (EMU) are classified into four types: sensitizers (type I), accumulators (type II), migrators (type III) and activators (type IV; Fig. 1e). A sensitizer ion is used to harvest pump photons and subsequently promote a neighbouring accumulator ion to excited states. A migrator ion extracts the excitation energy from high-lying energy states of the accumulator, followed by random energy hopping through the migrator ion sublattice and trapping of the migrating energy by an activator ion. To regulate energy exchange interaction between the accumulator and the activator, the sensitizer/accumulator and the activator are spatially confined in different layers of the core-shell structure, which is essential for eliminating deleterious cross-relaxation (vide infra). To generate an efficient EMU process, arrays of migrator ions through the core-shell interface are needed to bridge the energy transfer from the accumulator to the activator. A key feature of the EMU design is that the excitation energy collected by the sensitizer can be amassed in the accumulator by successive energy transfer while enabling one-step energy transfer to the activator. Thus, stringent selection rules for activators (type IV ion) can be largely exempted, in parallel with the benefit of the inherent high conversion efficiency of ETU for low energy excitation photons. The core-shell layout also allows a facile modulation in activator composition and concentration

while minimizing luminescence quenching. As a result, tunable upconversion emissions are likely to be realized for activators without long-lived intermediary energy states.

As a proof-of-concept experiment, we used a $\text{NaGdF}_4/\text{NaGdF}_4$ core-shell nanoparticle with the sensitizer/accumulator (Yb/Tm) and the activator (X^{3+} ; X = Tb, Eu, Dy or Sm) separately incorporated into the core and shell layer of the nanoparticle, respectively (Fig. 2a). Hexagonal phase NaGdF_4 was chosen as the host material for its ability to render high upconversion efficiency in addition to the benefit of using the Gd sublattice for fast energy migration⁴⁰. Importantly, the lowest excited level (${}^6\text{P}_{7/2}$) of Gd^{3+} is situated in the ultraviolet spectral region, where most of the lanthanide ions have overlapping absorption bands (Fig. 2b). As an added benefit, the ${}^6\text{P}_{7/2}$ state and ground state of Gd^{3+} are separated by a relatively large energy gap ($\sim 3.2 \times 10^4 \text{ cm}^{-1}$), leading to a minimized energy loss caused by multiphonon emission and cross-relaxation⁴³. The sensitizer/accumulator pair of Yb/Tm was used to accumulate the excitation photons. It is well established that efficient energy transfer occurring between these two ions can result in the population of the ${}^6\text{P}_{7/2}$ state of Gd^{3+} by accumulating more than five near-infrared photons (Fig. 2b; ref. 44).

In a typical procedure, NaGdF_4 nanoparticles co-doped with Yb/Tm were first fabricated and then used as seeds for epitaxial growth of NaGdF_4 shells comprising activators (Supplementary Figs S2 and S3). The hexagonal phase of the as-prepared core-shell nanoparticles was confirmed by high-resolution scanning

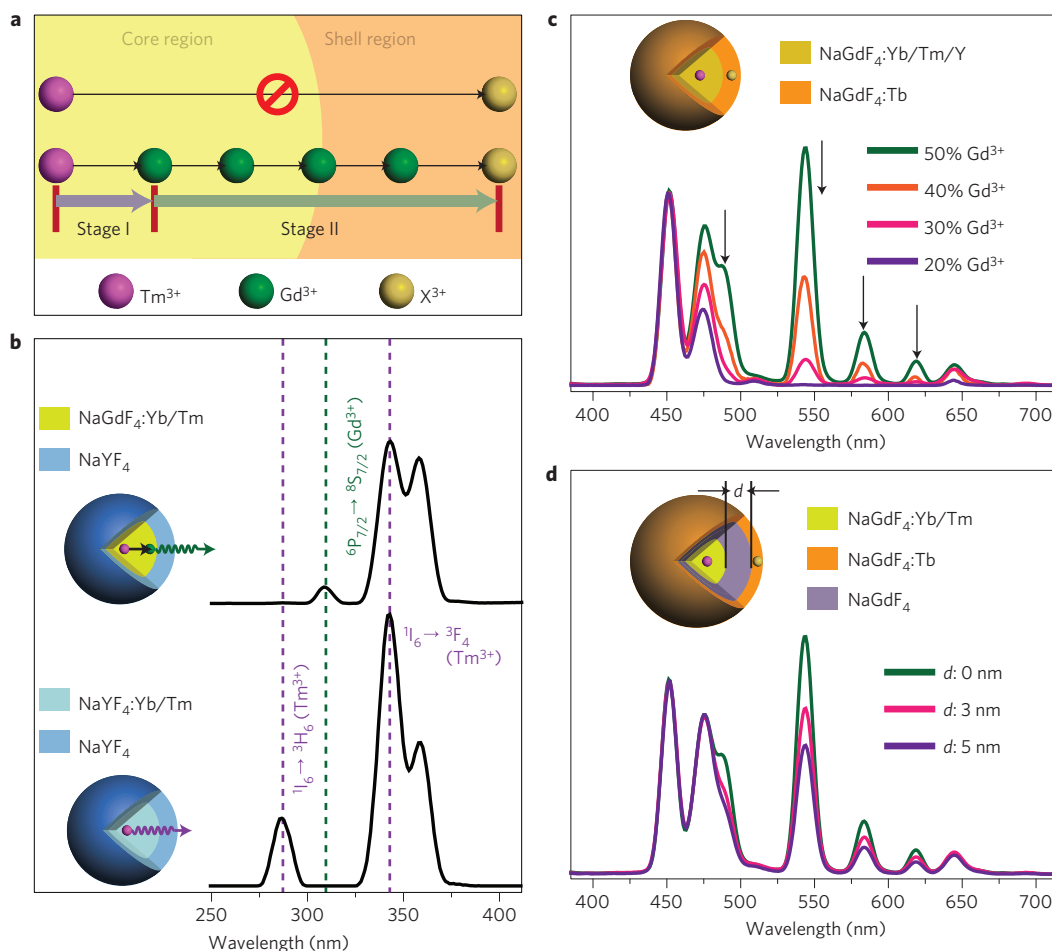


Figure 3 | Mechanistic investigation of the EMU process in core-shell nanoparticles. **a**, Scheme showing the Gd sublattice-mediated energy transfer from Tm^{3+} to the activator through the core-shell interface. **b**, Emission spectra of the nanoparticles in the ultraviolet spectral region showing the sensitized emission of Gd^{3+} by Tm^{3+} , supporting the existence of energy transfer from Tm^{3+} to Gd^{3+} . **c**, Emission spectra of the nanoparticles in the visible spectral region showing the suppressed Tb^{3+} emission at reduced Gd^{3+} concentrations in the core level, demonstrating the key role of the Gd sublattice in transferring the energy to the activator. **d**, Emission spectra of core-shell-shell nanoparticles with Tm^{3+} and Tb^{3+} separated by a NaGdF_4 shell layer of different thickness (0, 3, and 5 nm). The largely preserved Tb^{3+} emission for particles with a spacing layer of 5 nm indicates that energy migration through the Gd sublattice can travel a substantial length.

transmission electron microscopy (STEM; Fig. 2c,e). The STEM image of a single particle (~ 3 nm in shell thickness) shows a remarkable single-crystalline structure without noticeable defects at atomic resolution. Despite the high quality of the STEM image, as evidenced by the visibility of the light element Na (Fig. 2d), the core and the shell cannot be distinguished directly from the image by diffraction contrast or Z contrast because they have very close crystalline structures and compositions. However, electron energy-loss spectroscopy (EELS) analysis conducted on several randomly selected nanoparticles illustrated that the elemental distributions of the nanoparticles are very consistent with the designed compositions for the core-shell structures (Fig. 2f, Supplementary Figs S4 and S16). Photoluminescence investigation revealed that a collection of lanthanide ions including Tb^{3+} , Eu^{3+} , Dy^{3+} and Sm^{3+} can serve as the activator to generate tunable upconversion emissions spanning the visible spectral region (Fig. 2g). Significantly, all the emissions obtained are visible at room temperature at a moderate excitation density (15 W cm^{-2}). In stark contrast, conventional methods for generating anti-Stokes emissions on these activators require either a significantly higher excitation density (over 10^6 W cm^{-2}) or extremely low operating temperatures^{1,10}. This feature would add flexibility in designing multicolour particle labels for multiplexed imaging applications under single-wavelength

excitation (Fig. 2h). As an added benefit, the newly developed emitters (Tb^{3+} and Eu^{3+}) offer much longer luminescence lifetimes (Supplementary Fig. S7) than the accumulator (Tm^{3+}), providing opportunities for time-resolved optical studies⁴⁵.

The EMU process in the core-shell nanoparticles is strongly affected by the dopant concentration. For instance, an increase in activator concentration generally favours the trapping of the excitation energy of Gd^{3+} . However, elevated doping levels also induce deleterious cross-relaxation that quenches the luminescence. By correlating the emission intensity with the activator concentration and using the visible emission of Tm^{3+} as a reference, the optimum activator concentrations were determined to be 15, 15, 5 and 5 mol% for Tb^{3+} , Eu^{3+} , Dy^{3+} and Sm^{3+} , respectively (Supplementary Fig. S6). Furthermore, optimized dopant concentrations for Yb^{3+} and Tm^{3+} have been determined to be 49 and 1 mol% for generating maximum Tm^{3+} emission to populate the ${}^6\text{P}_{7/2}$ state of Gd^{3+} (Supplementary Fig. S5). We have compared our samples with a common upconversion reference in the form of $\text{NaYF}_4:\text{Yb}/\text{Er}$ nanoparticles to estimate the relative emission efficiency. With optimized dopant concentrations, the $\text{NaGdF}_4:\text{Yb}/\text{Tm}@/\text{NaGdF}_4:\text{X}$ nanoparticles showed an emission intensity of 1.2 ($\text{X} = \text{Tb}$), 1.3 ($\text{X} = \text{Eu}$), 0.19 ($\text{X} = \text{Dy}$) and 0.13 ($\text{X} = \text{Sm}$) times the intensity of typical $\text{NaYF}_4:\text{Yb}/\text{Er}@/\text{NaYF}_4$ nanoparticles (~ 30 nm).

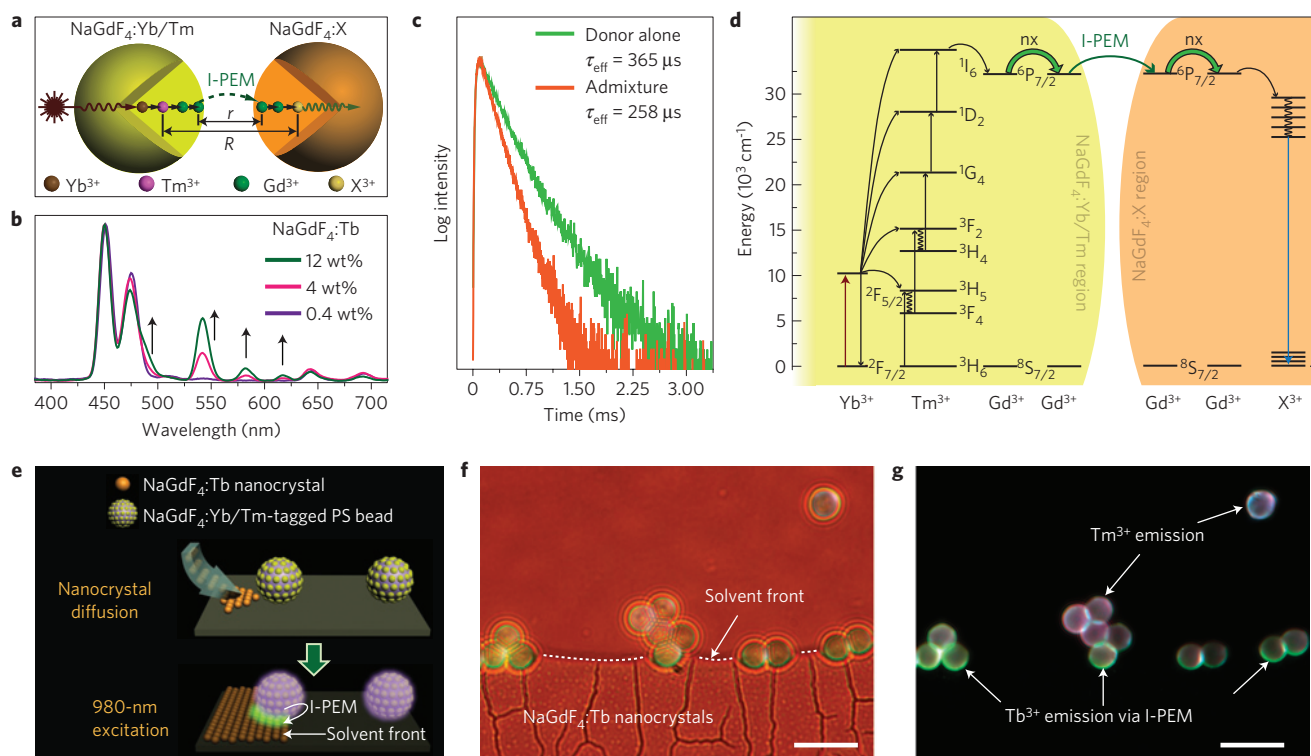


Figure 4 | Effect of energy transfer between nanoparticles by means of energy migration. **a**, Schematic design of I-PEM between the NaGdF₄:Yb/Tm and NaGdF₄:X nanoparticles (X: activator ion). **b**, Emission spectra of ethanol/water solutions containing NaGdF₄:Yb/Tm nanoparticles (2 wt%) and NaGdF₄:Tb nanoparticles of varying concentrations. **c**, Upconversion luminescence decay curves of Gd³⁺ emission at 310 nm in NaGdF₄:Yb/Tm (49/1 mol%) and in a binary mixture (1:1; wt/wt) of NaGdF₄:Yb/Tm (49/1 mol%) and NaGdF₄:Tb (15 mol%), respectively. **d**, Proposed energy transfer mechanism between NaGdF₄:Yb/Tm and NaGdF₄:X nanoparticles. **e**, Schematic design for visualizing the I-PEM process. The NaGdF₄:Yb/Tm nanoparticles were attached to polystyrene beads for signal amplification. **f, g**, Micrographs of the nanoparticle-tagged polystyrene beads under dual-mode (halogen light and 980-nm laser) illumination and 980-nm excitation alone, respectively. Scale bars, 10 μm.

To confirm the need of a core–shell structure that separates the Yb/Tm pair and the activator for efficient EMU, we doped Tb³⁺ homogeneously with the Yb³⁺ and Tm³⁺ in the NaGdF₄ host lattice. The control experiments showed that both Tm³⁺ and Tb³⁺ emissions are largely quenched, possibly caused by the cross-relaxation between the Yb/Tm and the Tb³⁺ (Supplementary Fig. S10). Similar quenching effects have also been observed for nanoparticles with Eu³⁺, Dy³⁺ and Sm³⁺ activators doped homogeneously with the Yb/Tm pair (Supplementary Fig. S11).

The Gd sublattice-mediated energy exchange in core–shell nanoparticles (Fig. 3a) was supported by the observations that Tb³⁺ only promotes the time decay of Gd³⁺ emission while its emission intensity exhibits a similar dependence on pump power to that of Tm³⁺ at 290 nm (Supplementary Fig. S12). In a further attempt to probe energy transfer from Tm³⁺ to Gd³⁺ in the EMU process (Stage I, Fig. 3a), we prepared NaGdF₄:Yb/Tm nanoparticles coated with an optically inert layer of NaYF₄ (Supplementary Fig. S13), which prevents the excitation energy of Gd³⁺ from trapping by surface quenching sites. As anticipated, we observed Gd³⁺ emission at ~310 nm (⁶P_{7/2} → ⁸S_{7/2}), clearly indicating the existence of excited Gd³⁺ states (Fig. 3B). When we replaced the Gd³⁺ in the core level with optically inactive Y³⁺, recovered upconversion emission of Tm³⁺ was observed at ~290 nm (¹I₆ → ³H₆), further supporting the existence of energy transfer from the Tm³⁺ to Gd³⁺ (Fig. 3b).

To verify the critical role of the Gd sublattice in mediating energy migration and subsequent transfer to the activator (Stage II, Fig. 3a), we assessed a series of core–shell nanoparticles with varied Gd³⁺ content in the core level (Supplementary Fig. S17). The Gd³⁺ in the core sublattice was partially replaced by optically inactive Y³⁺ (0–30 mol%). With decreasing Gd³⁺ concentration (50–20 mol%),

a gradual decrease in emission intensity was observed for the activator (Fig. 3c). The decrease in the emission intensity can be attributed to the suppression of the energy migration process by virtue of the increased Gd–Gd interionic distance. We noted that 30 mol% of Gd³⁺ is required to initiate the energy transfer from Tm³⁺ to the activator (Fig. 3c). From the photoluminescence data and crystallographic structure of the Gd sublattice, we derived a critical energy transfer distance (*d_c*) of ~6 Å between Gd³⁺ ions (Supplementary Fig. S15). The short distance indicates that the Gd–Gd energy transfer is dominated by exchange interaction, which is in agreement with literature⁴⁰. Together, these results provide clear evidence that the activator is excited via energy migration through the Gd sublattice.

Another prominent feature of the EMU process is that the migration of excitation energy through the Gd sublattice can travel a substantial length. To shed more light on this effect, we prepared NaGdF₄@NaGdF₄@NaGdF₄ core–shell–shell nanoparticles with different inner shell thicknesses (Supplementary Fig. S19). The Yb/Tm pair and the activator were selectively doped into the core and outermost shell layer, respectively. Despite having a 5-nm spacing layer of NaGdF₄, the emission of Tb³⁺ activator is essentially preserved (Fig. 3d). The results further exclude the possibility of activator excitation by direct energy transfer from Tm³⁺, which otherwise would follow an inverse sixth power dependence on distance. The slight decline in emission intensity of Tb³⁺ relative to that of Tm³⁺ is mainly due to dissipation of the excitation energy over long-distance migration, which spans approximately 28 Gd atomic layers along the *c*-axis (Supplementary Fig. S15).

The EMU process in core–shell nanoparticles, investigated with four types of lanthanide ions incorporated in different layers,

can be realized across two sets of NaGdF₄ nanoparticles having different dopants. One set of particles doped with the Yb/Tm pair are used as energy donors, whereas the other set doped only with different activators act as energy acceptors (Fig. 4a). On near-infrared excitation, we envisage that the excitation energy, carried by the Gd sublattice in a donor particle, can be transferred to the Gd³⁺ ions in an adjacent acceptor particle through inter-particle energy migration (I-PEM). Further energy migration by the Gd sublattice in the acceptor particle and subsequent trapping by the activator could lead to the emission from the acceptor particle.

To validate our hypothesis, NaGdF₄:Yb/Tm and NaGdF₄:Tb nanoparticles were prepared and mixed at different molar ratios in ethanol/water (4:1; v/v) solutions. Note that surface oleate ligands were removed using a strong acid to reduce depletion of excitation energy at the particle interface (Supplementary Figs S21 and S22). Following near-infrared excitation, the energy transfer between the nanoparticles is evident, as determined by sensitized Tb³⁺ emission from particle solutions (Fig. 4b). Notably, the emission intensity of Tb³⁺ increased with increasing concentration of acceptor particles. The removal of oleate ligands also recovered the radiative transitions of Gd³⁺ at ~310 nm (⁶P_{7/2} → ⁸S_{7/2}) to some extent. The time decay study revealed a shortening in the lifetime of Gd³⁺ emission at 310 nm on admixing with the acceptor particles (Fig. 4c), whereas decay rates of Tm³⁺ remained essentially unaltered (Supplementary Fig. S24). In further control experiments with Gd³⁺ ions in the donor particles replaced by optically inactive Y³⁺, no Tb³⁺ emission was observed (Supplementary Fig. S25). Therefore, the excitation of Tb³⁺ can be clearly ascribed to a Gd sublattice-mediated I-PEM process (Fig. 4d). Remarkably, by organizing donor and acceptor particles in close proximity on a solid substrate by using donor-modified polystyrene beads (3.55 μm), the I-PEM process can be directly visualized at the point of contact between the donor and acceptor particles under luminescence microscopy (Fig. 4e–g).

The optical properties observed in these nanoparticles are especially surprising because they have provided the first observation of inter-particle energy transfer with lanthanide-doped nanophosphors as energy acceptors (emitters). In contrast to quantum dots and organic dyes^{46,47}, lanthanide-doped nanophosphors typically feature several orders of magnitude smaller absorption cross-sections (~10⁻²¹ cm²) in the ultraviolet–visible spectral region, making them unsuitable as acceptors for conventional Förster resonance energy transfer (FRET) studies⁴⁸. The striking optical phenomenon described here would be dominated by the network of the Gd sublattice, which has the dual ability to shorten the interaction distance (from *R* to *r*) between the donor and the acceptor and to tune the mismatched energy levels to the same resonant frequency (Fig. 4a,d).

The successful control of energy transfer within a core–shell nanoparticle prompted us to design and fabricate luminescent materials exhibiting exciting optical properties. For example, we developed a synthesis for core–shell–shell structures with the capability to encode dual activators. In response to near-infrared excitation, the nanoparticles are able to emit light that covers almost the entire visible spectral range (Supplementary Fig. S27). With a single set of dually activated nanoparticles as energy donors, we further demonstrated simultaneous excitation of two different dyes by conventional FRET (Supplementary Fig. S28). By adopting the core–shell design, tunable upconversion emissions through the migration of excitation energy can also be achieved for the LiGdF₄ nanoparticle system (Supplementary Fig. S29).

The ability to tune upconversion properties for a rather wide range of activators by using a combination of energy migration and core–shell structural engineering would expand the range of applications for lanthanide-doped nanoparticles. When one considers the advantage and versatility offered by these nanoparticles, including non-blinking characteristics, the findings

of this study should have important implications for advanced bioimaging as they highlight the possibility of constructing novel luminescent nanoparticles with high designability and tunability. Given the substantial flexibility in manipulating energy transfer in nanostructures, our discovery may also stimulate new concepts on lanthanide-based luminescent materials.

Methods

Nanoparticle synthesis. We synthesized the lanthanide-doped NaGdF₄ nanoparticles using the method of ref. 25. Additional experimental details are provided in the Supplementary Information.

Scanning transmission electron microscopy. High-resolution STEM and EELS were performed on an FEI aberration-corrected Titan Cubed S-Twin transmission electron microscope operated at 200 kV. A probe Cs corrector was applied to get better spatial resolution. In a typical experiment, high-resolution STEM imaging was conducted at a 2-μs/pixel scanning rate with 70 μm C2 aperture, spot size 9, a high-angle annular dark-field (HAADF) detector, and 146 mm camera length. Under such conditions a spatial resolution of ~1.0 Å was obtained. EELS point analysis was performed with 150 μm C2 aperture, spot size 6, 29.6 mm camera length, 5 mm entrance aperture (collection angle β = 54 mrad) and 1 s collection time, whereas the EELS line scan was conducted using 70 μm C2 aperture, spot size 9, 29.6 mm camera length, 5 mm entrance aperture (collection angle β = 54 mrad) and 0.1 s/pixel collection time.

Luminescence spectroscopy and microscopy. Photoluminescence spectra were recorded at room temperature with a DM1501 monochromator equipped with a R928 photon counting photomultiplier tube (PMT), in conjunction with a 980-nm diode laser. The decay curves were measured with a customized ultraviolet to mid-infrared phosphorescence lifetime spectrometer (FSP920-C, Edinburgh) equipped with a digital oscilloscope (TDS3052B, Tektronix) and a tunable mid-band OPO laser as an excitation source (410–2,400 nm, Vibrant 355II, OPOTEK). Upconversion luminescence microscopy imaging was performed on an Olympus BX51 microscope with the xenon lamp adapted to a diode laser. Luminescence micrographs were recorded with a Nikon DS-R1i imaging system.

Received 15 July 2011; accepted 17 September 2011;
published online 23 October 2011

References

- Auzel, F. Upconversion and anti-Stokes processes with f and d ions in solids. *Chem. Rev.* **104**, 139–173 (2004).
- Downing, E., Hesselink, L., Ralston, J. & Macfarlane, R. A three-color, solid-state, three-dimensional display. *Science* **273**, 1185–1189 (1996).
- Cohen, B. E. Beyond fluorescence. *Nature* **467**, 407–408 (2010).
- van der Ende, B. M., Aartsa, L. & Meijerink, A. Lanthanide ions as spectral converters for solar cells. *Phys. Chem. Chem. Phys.* **11**, 11081–11095 (2009).
- Wang, G., Peng, Q. & Li, Y. Lanthanide-doped nanocrystals: Synthesis, optical-magnetic properties, and applications. *Acc. Chem. Res.* **44**, 322–332 (2011).
- Kaiser, W. & Garrett, C. G. B. Two-photon excitation in CaF₂:Eu²⁺. *Phys. Rev. Lett.* **7**, 229–231 (1961).
- Larson, D. R. *et al.* Water-soluble quantum dots for multiphoton fluorescence imaging *in vivo*. *Science* **300**, 1434–1436 (2003).
- Franken, P. A., Hill, A. E., Peters, C. W. & Weinreich, G. Generation of optical harmonics. *Phys. Rev. Lett.* **7**, 118–119 (1961).
- Pantazis, P., Maloney, J., Wu, D. & Fraser, S. E. Second harmonic generating (SHG) nanoprobes for *in vivo* imaging. *Proc. Natl Acad. Sci. USA* **107**, 14535–14540 (2010).
- Suyver, J. F. *et al.* Novel materials doped with trivalent lanthanides and transition metal ions showing near-infrared to visible photon upconversion. *Opt. Mater.* **27**, 1111–1130 (2005).
- Wang, F. & Liu, X. Recent advances in the chemistry of lanthanide-doped upconversion nanocrystals. *Chem. Soc. Rev.* **38**, 976–989 (2009).
- Chatterjee, D. K., Gnanasammandhan, M. K. & Zhang, Y. Small upconverting fluorescent nanoparticles for biomedical applications. *Small* **24**, 2781–2795 (2010).
- Bünzli, J.-C. G. Lanthanide luminescence for biomedical analyses and imaging. *Chem. Rev.* **110**, 2729–2755 (2010).
- Li, C. & Lin, J. Rare earth fluorides nano-/microcrystals: Synthesis, surface modification and application. *J. Mater. Chem.* **20**, 6831–6847 (2010).
- Haase, M. & Schäfer, H. Upconverting nanoparticles. *Angew. Chem. Int. Ed.* **50**, 5808–5829 (2011).
- Wang, X., Zhuang, J., Peng, Q. & Li, Y. A general strategy for nanocrystal synthesis. *Nature* **437**, 121–124 (2005).
- Mai, H. *et al.* High-quality sodium rare-earth fluoride nanoparticles: Controlled synthesis and optical properties. *J. Am. Chem. Soc.* **128**, 6426–6436 (2006).

18. Feng, W., Sun, L. D. & Yan, C. H. Ag nanowires enhanced upconversion emission of NaYF₄:Yb, Er nanocrystals via a direct assembly method. *Chem. Commun.* 4393–4395 (2009).
19. Schäfer, H., Ptacek, P., Eickmeier, H. & Haase, M. Synthesis of hexagonal Yb³⁺, Er³⁺-doped NaYF₄ nanocrystals at low temperature. *Adv. Funct. Mater.* **19**, 3091–3097 (2009).
20. Wang, M. *et al.* Immunolabeling and NIR-excited fluorescent imaging of HeLa cells by using NaYF₄:Yb, Er upconversion nanoparticles. *ACS Nano* **3**, 1580–1586 (2009).
21. Wu, S. *et al.* Non-blinking and photostable upconverted luminescence from single lanthanide-doped nanocrystals. *Proc. Natl Acad. Sci. USA* **106**, 10917–10921 (2009).
22. Zhang, F. *et al.* Fabrication of Ag@SiO₂@Y₂O₃:Er nanostructures for bioimaging: Tuning of the upconversion fluorescence with silver nanoparticles. *J. Am. Chem. Soc.* **132**, 2850–2851 (2010).
23. Boyer, J.-C., Carling, C.-J., Gates, B. D. & Branda, N. R. Two-way photoswitching using one type of near-infrared light, upconverting nanoparticles, and changing only the light intensity. *J. Am. Chem. Soc.* **132**, 15766–15772 (2010).
24. Wang, F. *et al.* Simultaneous phase and size control of upconversion nanocrystals through lanthanide doping. *Nature* **463**, 1061–1065 (2010).
25. Wang, F., Wang, J. & Liu, X. Direct evidence of a surface quenching effect on size-dependent luminescence of upconversion nanoparticles. *Angew. Chem. Int. Ed.* **49**, 7456–7460 (2010).
26. Liu, Y. *et al.* A strategy to achieve efficient dual-mode luminescence of Eu³⁺ in lanthanides doped multifunctional NaGdF₄ nanocrystals. *Adv. Mater.* **22**, 3266–3271 (2010).
27. Ye, X. *et al.* Morphologically controlled synthesis of colloidal upconversion nanophosphors and their shape-directed self-assembly. *Proc. Natl Acad. Sci. USA* **107**, 22430–22435 (2010).
28. Abel, K. A., Boyer, J. C., Andrei, C. M. & van Veggel, F. C. J. M. Analysis of the shell thickness distribution on NaYF₄/NaGdF₄ core/shell nanoparticles by EELS and EDS. *J. Phys. Chem. Lett.* **2**, 185–189 (2011).
29. Bogdan, N., Vetrone, F., Ozin, G. A. & Capobianco, J. A. Synthesis of ligand-free colloidal stable water dispersible brightly luminescent lanthanide-doped upconverting nanoparticles. *Nano Lett.* **11**, 835–840 (2011).
30. Chen, G., Ohulchanskyy, T. Y., Kumar, R., Agren, H. & Prasad, P. N. Ultrasmall monodisperse NaYF₄:Yb³⁺/Tm³⁺ nanocrystals with enhanced near-infrared to near-infrared upconversion photoluminescence. *ACS Nano* **4**, 3163–3168 (2010).
31. Mader, H. S., Kele, P., Saleh, S. M. & Wofbeis, O. S. Upconverting luminescent nanoparticles for use in bioconjugation and bioimaging. *Curr. Opin. Chem. Biol.* **14**, 582–596 (2010).
32. DiMaio, J. R., Sabatier, C., Kokuoz, B. & Ballato, J. Controlling energy transfer between multiple dopants within a single nanoparticle. *Proc. Natl Acad. Sci. USA* **105**, 1809–1813 (2008).
33. Zhou, J. *et al.* Fluorine-18-labeled Gd³⁺/Yb³⁺/Er³⁺ codoped NaYF₄ nanophosphors for multimodality PET/MR/UCL imaging. *Biomaterials* **32**, 1148–1156 (2011).
34. Liu, Q. *et al.* ¹⁸F-labeled magnetic-upconversion nanophosphors via rare-earth cation-assisted ligand assembly. *ACS Nano* **5**, 3146–3157 (2011).
35. Schietinger, S., Aichele, T., Wang, H., Nann, T. & Benson, O. Plasmon-enhanced upconversion in single NaYF₄:Yb³⁺/Er³⁺ codoped nanocrystals. *Nano Lett.* **10**, 134–138 (2010).
36. Chen, D. *et al.* Modifying the size and shape of monodisperse bifunctional alkaline-earth fluoride nanocrystals through lanthanide doping. *J. Am. Chem. Soc.* **132**, 9976–9978 (2010).
37. Yi, G. S. & Chow, G. M. Synthesis of hexagonal-phase NaYF₄:Yb, Er and NaYF₄:Yb, Tm nanocrystals with efficient up-conversion fluorescence. *Adv. Funct. Mater.* **16**, 2324–2329 (2006).
38. Zhang, H. *et al.* Plasmonic modulation of the upconversion fluorescence in NaYF₄:Yb/Tm hexaplate nanocrystals using gold nanoparticles or nanoshells. *Angew. Chem. Int. Ed.* **49**, 2865–2868 (2010).
39. Xue, X., Wang, F. & Liu, X. Emerging functional nanomaterials for therapeutics. *J. Mater. Chem.* **21**, 13107–13127 (2011).
40. Blasse, G. The physics of new luminescent materials. *Mater. Chem. Phys.* **16**, 201–236 (1987).
41. Chua, M. & Tanner, P. A. Energy transfer and migration in highly forbidden transitions of lanthanide ion doped crystals. *Chem. Phys.* **250**, 267–278 (1999).
42. Kutsenko, A. B., Heber, J., Kapphan, S. E., Demirbilek, R. & Zakharchenya, R. I. Energy migration and energy transfer processes in RE³⁺ doped nanocrystalline yttrium oxide. *Phys. Status Solidi c* **2**, 685–688 (2005).
43. Wegh, R. T., Donker, H., Oskam, K. D. & Meijerink, A. Visible quantum cutting in LiGdF₄:Eu³⁺ through downconversion. *Science* **283**, 663–666 (1999).
44. Qin, W. *et al.* Ultraviolet upconversion fluorescence from ⁶D₁ of Gd³⁺ induced by 980 nm excitation. *Opt. Lett.* **33**, 2167–2169 (2008).
45. Tu, D. *et al.* Time-resolved FRET biosensor based on amine-functionalized lanthanide-doped NaYF₄ nanocrystals. *Angew. Chem. Int. Ed.* **50**, 6306–6310 (2011).
46. Bruchez, M. Jr, Moronne, M., Gin, P., Weiss, S. & Alivisatos, A. P. Semiconductor nanoparticles as fluorescent biological labels. *Science* **281**, 2013–2016 (1998).
47. Binnemans, K. Lanthanide-based luminescent hybrid materials. *Chem. Rev.* **109**, 4283–4374 (2009).
48. Jares-Erijman, E. A. & Jovin, T. M. FRET imaging. *Nature Biotechnol.* **21**, 1387–1395 (2003).

Acknowledgements

The bulk of the work was supported by the Singapore Ministry of Education (No. MOE2010T2-1-083), the Singapore-MIT Alliance, and the Agency for Science, Technology and Research (No. IMRE/11-1C0110). Y.H. is grateful to KAUST Global Collaborative Research for the Academic Excellence Alliance (AEA) fund. H.Z. and X.C. acknowledge the financial support from the NSFC (Nos. 10974200 and 51002151) and the 863 programs of MOST (Nos. 2009AA03Z430 and 2011AA03A407). We thank T. Nguyen, Y. Liu and L. Tan for their help in sample characterization.

Author contributions

F.W. and X.L. conceived the experiments and wrote the paper. F.W., R.D. and J.W. were primarily responsible for the experiments. Q.W. and Y.H. performed the STEM, EDX and EELS characterizations. H.Z. and X.C. carried out the time-decay measurements. All authors contributed to the analysis of this manuscript.

Additional information

The authors declare no competing financial interests. Supplementary information accompanies this paper on www.nature.com/naturematerials. Reprints and permissions information is available online at <http://www.nature.com/reprints>. Correspondence and requests for materials should be addressed to X.L.